Supporting Information

Mishra et al. 10.1073/pnas.1200949109

SI Text

Experimental Methods. The experimental setup is shown in Figs. S1 and S2. Nitrogen gas saturated with $HNO_{3(g)}$ by sparging a 2.25-M aqueous solution of HNO_3 (or DNO_3) maintained at 278 K was introduced into the chamber of the electrospray mass spectrometer (ESMS), where it collided with liquid microjets of variable compositions. The concentration of $HNO_{3(g)}$ in the saturated nitrogen gas was calculated by using reported partial vapor pressures above H_2O/HNO_3 solutions (1, 2). We assumed a similar liquid-vapor diagram for DNO_3 solutions. Typical experimental conditions were: drying gas flow rate, 10 L min^{-1}; drying gas temperature, 340 °C; inlet voltage, -3.5 kV relative to ground; fragmentor voltage, 26 V. HNO_3 (69%; Sigma-Aldrich) and DNO_3 (D, 99%, 65–70% in D_2O; Cambridge Isotope Laboratories) were used as received. All solutions were prepared in purified water (resistivity, 18.2 MΩ cm) from a Millipore Milli-Q gradient water-purification system. Solution pH_{BLK} was adjusted by adding concentrated HCl or NaOH solutions and measured with a calibrated pH meter (VWR). Selective adsorption of OH$^-$ on the stainless steel walls was observed by Duffin and Saykally (3) in a similar setup, which led to the ejection of an acidic liquid jet. We have independent evidence that our jets, in contrast, are not acidic (4). It should be emphasized, however, that the velocity at which the liquid jet emerges from the nozzle is approximately 500 times slower than that required for observing electrokinetic effects in our experiments (3).

Computational Methods. Energy-optimized water decamers, W_{10}, consisting of overlapping five-membered rings have been shown to be most stable isomers (5, 6). In this configuration each water molecule is hydrogen-bonded to three neighbors (7, 8). Nitric acid binds to W_{10} into optimized $(W_{10} \cdot HNO_3)$ adducts via two hydrogen bonds with the release of $\Delta H^0 = -13.0$ kcal/mol and $\Delta G^0 = -1.2$ kcal/mol (Fig. 3A). The insertion of a chloride into W_{10} leads to a relaxed $(Cl \cdot W_{10})^-$ structure in which Cl$^-$ emerges to the surface of the cluster and is hydrogen-bonded to the water molecules of one of the rings (Fig. 3B) (9). The decreased Mulliken electron population (-0.65 vs. -1 e^-) on chloride in $(Cl \cdot W_{10})^-$ reveals that the surrounding waters have become better proton acceptors via electron density delocalization.

Calculations of nitric acid interactions with W_{10} and $(Cl \cdot W_{10})^-$ clusters were initialized by positioning a nitric acid molecule close to one of the waters of the W_{10} rings, and to the five waters nearest to chloride in $(Cl \cdot W_{10})^-$ (Fig. 3B). Product structures created out of the three lowest-energy adducts by separating the proton from nitrate with none, one, or two waters were then energy-minimized. We found stable zwitterion products separated by one and two waters in the presence of chloride, and by two waters in its absence. The lowest-energy products in each case correspond to ion pairs separated by two waters. Transition states (TS) for transforming adducts into stable products were then searched by optimizing structures in which the six O—H bonds connecting nitrate with hydronium were constrained until the chosen set of constraints led to an imaginary frequency vibration. The path of steepest ascent was then followed by tracking the eigenvector of the motion associated with the imaginary frequency until an energy maximum was found. Full Hessian harmonic calculations were then performed for the TS structures. We also investigated whether nitric acid would transfer a proton through, rather than assisted by, chloride. Structures in which nitric acid was hydrogen-bonded or fully transferred its proton to chloride were found to lie G = 1.6 kcal/mol (H = 4.1 kcal/

mol) and G = 9.0 kcal/mol (H = 8.38 kcal/mol) above the aforementioned lowest-energy adduct. Thus, chloride rather than relaying proton transfer assists in this system.

Results. From the frequency of HNO_3 collisions on water's surface given by the kinetic theory of gases [$f(cm^{-2} s^{-1}) = 1/4 \ \gamma c \ n$ ($\gamma \approx 1$ is the reactive uptake coefficient; $c = 3.2 \times 10^4$ cm s^{-1} is the mean speed of HNO_3 molecules at 300 K, and n their number density in molecules cm^{-3})] (10, 11), we deduce that $f \times (\tau/\Delta) = 1.9 \times 10^{18}$ protons cm$^{-3} = 10^{-2.5}$ M must be delivered to interfacial layers of thickness Δ[cm] upon exposure to $n = 3.3 \times 10^{12}$ $HNO_{3(g)}$ molecules cm^{-3} during τ[s] contact times—i.e., $(\Delta/\tau) = 0.014$ cm s^{-1}. Previous experiments have shown that τ is approximately 10 μs (11). Thus, we estimate that the thickness of the interfacial layers sampled in our experiments is $\Delta \sim 1.4 \times 10^{-7}$ cm.

In Fig. 2 A and B, the ratios $\alpha = I_{117}/I_{118} = PCOOH_2^+/PCOOHD^+$, $\beta = I_{118}/I_{119} = PCOOHD^+/PCOOD_2^+$ report the H/D composition of the interfacial layers of 1-mM PCOOH in $1:1/D_2O:H_2O$ microjets exposed to either $HNO_{3(g)}$ or $DNO_{3(g)}$. The statistical protonation/deuteration (hydronation) of PCOO$^-$ in interfacial layers of proton molar fraction x_H leads to: $\alpha = \frac{x_H}{2(1-x_H)}$; $\beta = \frac{2x_H}{1-x_H}$. From the asymptotic ratios ($\alpha = 1.92$, $\beta = 6.0$) measured under $(HNO_{3(g)}) > 7 \times 10^{12}$ molecules cm^{-3}, we derive: $x_H = 0.77 \pm 0.02$. Similarly, from $\alpha = 0.93$, $\beta = 3.4$, under $(DNO_{3(g)}) > 6 \times 10^{12}$ molecules cm^{-3}, we obtain: $x_H = 0.64 \pm 0.01$. As a reference, the $\alpha = 1.31$ ratio measured in 1-mM PCOOH in $1:1/H_2O:D_2O$ pH 3.0 microjets not exposed to gaseous nitric corresponds to $x_H^0 = 0.72$ (rather than $x_H^0 = 0.50$). Therefore, the fraction of protons in interfacial layers increases from $x_H^0 = 0.72$ to $x_H = 0.77$ under $HNO_{3(g)}$ and decreases to $x_H = 0.64$ under $DNO_{3(g)}$. Because x_H^0 is perturbed to similar but opposite extents (by $\pm 9\%$ on average) upon exposure to $HNO_{3(g)}$ or $DNO_{3(g)}$, we infer (*i*) a small kinetic isotope effect for the interfacial dissociation of $H(D)NO_{3(g)}$, and (*ii*) an approximately 90% contribution by the $1:1/D_2O:H_2O$ solvent to the isotopic composition of interfacial layers under present experimental conditions. Because approximately 0.6-mM hydrons are delivered under $n = 7 \times 10^{12} H(D)NO_{3(g)}$ molecules cm^{-3}, we infer that the effective water concentration in the interfacial layers is approximately 0.03 M.

Discussion. Consider a disk of interfacial water of radius R_S, depth $\Delta = 1.4 \times 10^{-7}$ cm (see *SI Results*), and volume $V_S = \pi R_S^2 \Delta$, centered at a chloride ion. At 30 μM (by assuming uniform concentration throughout) there is 1 Cl$^-$ per $N_W = 2 \times 10^6$ H_2O molecules of volume $V_W = 3 \times 10^{-23}$ cm^3. Therefore, $R_S = (V_W \times N_W \times \Delta^{-1} \times \pi^{-1})^{1/2} = 117$ nm. Thus, a HNO_3 molecule hitting the surface of a >30-μM solution will have to diffuse on average $R_S < 1.2 \times 10^{-5}$ cm to reach a Cl$^-$ and undergo barrierless dissociation. By assuming that the frequency of diffusional jumps between surface wells of depth E_D can be estimated from transition state theory as ν_D (s^{-1}) approximately $10^{13} \exp(-E_D/k_BT)$, we obtain: ν_D approximately 7×10^{10} s^{-1}, with $E_D \sim 3$ kcal mol^{-1} at 300 K. The time to make 376 jumps of length 3×10^{-8} cm to cover the distance $R_S = 1.2 \times 10^{-5}$ cm is therefore $376/\nu_D$ approximately 5 nanoseconds, which is comparable to the residence time of adsorbed gases on the surface of water (11).

1. Brimblecombe P, Clegg SL (1990) Equilibrium partial pressures of strong acids over concentrated solutions. 3. The temperature variations of HNO_3 solubility. *Atmos Environ A* 24:1945–1955.
2. Tang IN, Munkelwitz HR, Lee JH (1988) Vapor liquid equilibrium measurements for dilute nitric-acid solutions. *Atmos Environ* 22:2579–2585.
3. Duffin AM, Saykally RJ (2007) Electrokinetic hydrogen generation from liquid water microjets. *J Phys Chem C* 111:12031–12037.
4. Mishra H, Enami S, Hoffmann MR, Colussi AJ (2012) Bronsted basicity of the air-water interface, in press.
5. Xu X, Goddard WA (2004) Bonding properties of the water dimer: A comparative study of density functional theories. *J Phys Chem A* 108:2305–2313.
6. Xu X, Goddard WA (2004) The X3LYP extended density functional for accurate descriptions of nonbond interactions, spin states, and thermochemical properties. *Proc Natl Acad Sci USA* 101:2673–2677.
7. Su JT, Xu X, Goddard WA (2004) Accurate energies and structures for large water clusters using the X3LYP hybrid density functional. *J Phys Chem A* 108:10518–10526.
8. Shields RM, Temelso B, Archer KA, Morrell TE, Shields GC (2010) Accurate predictions of water cluster formation, $(H_2O)_{n=2-10}$. *J Phys Chem A* 114:11725–11737.
9. Francl MM, et al. (1982) Self-consistent molecular-orbital methods. 23. A polarization-type basis set for 2nd-row elements. *J Chem Phys* 77:3654–3665.
10. Davidovits P, Kolb CE, Williams LR, Jayne JT, Worsnop DR (2006) Mass accommodation and chemical reactions at gas-liquid interfaces. *Chem Rev* 106:1323–1354.
11. Enami S, Hoffmann MR, Colussi AJ (2010) Proton availability at the air/water interface. *J Phys Chem Lett* 1:1599–1604.
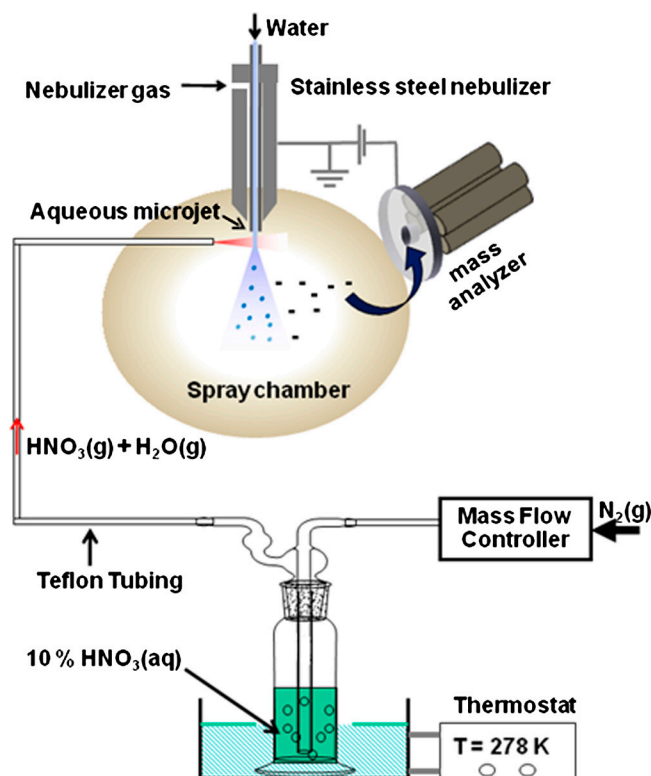
Fig. S1. Schematic diagram of the experimental setup. A microjet is created in the spraying chamber of an ESM spectrometer by injecting water through an electrically grounded stainless steel nebulizer (100-μm internal diameter) and briefly exposed to nitric acid vapors before it is broken up (after approximately 10 microseconds) into charged droplets by the nebulizer gas. After subsequent solvent evaporation and successive Coulomb explosions, excess ion are ultimately ejected to the gas-phase via field desorption and detected by mass spectrometry in <1 millisecond. The spray chamber is at 1 atm of N_2, 293 K throughout.
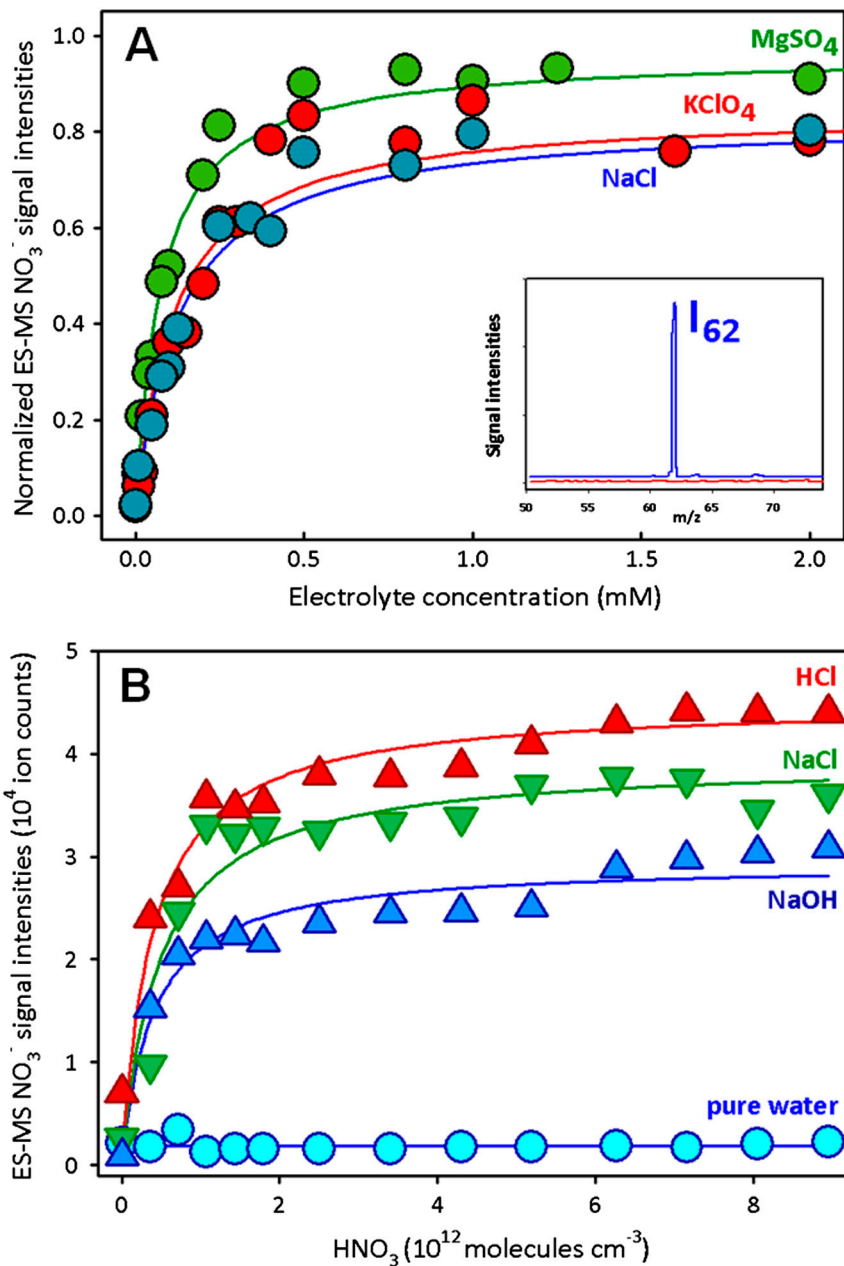
Fig. S2. Functional diagram of our ESMS experimental setup.

Fig. S3. (*A*) Electrospray mass spectral nitrate signal intensities (I_{62}) detected on aqueous $MgSO_4$, $KClO_4$, or NaCl microjets exposed to 3×10^{12} molecules cm^{-3} of gaseous nitric acid for approximately 10 μs as functions of electrolyte concentration. Solid curves fit experimental data with Langmuir adsorption functions: $I_{62} = I_{62}^{max}[\text{electrolyte}] \times (K_{1/2} + [\text{electrolyte}])^{-1}$; $K_{1/2}$ = 77 μM ($MgSO_4$), 117 μM ($KClO_4$), and 128 μM (NaCl). *Inset* shows ES mass spectra (signal intensities in arbitrary units) on deionized water (red) and 1-mM NaCl (blue). All experiments under 1 atm of N_2 at 293 K. (*B*) Electrospray mass spectral nitrate signals (m/z = 62) detected on pure water, and on 1-mM HCl, NaCl, or NaOH microjets exposed to gaseous nitric acid for approximately 10 μs as a function of $HNO_{3(g)}$ concentration. All experiments in 1 atm of N_2 at 293 K.

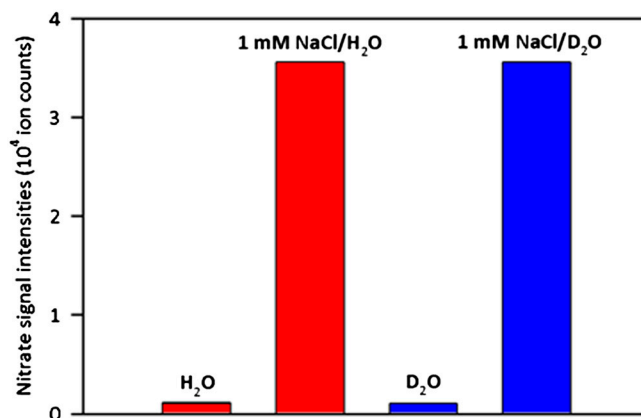**Fig. S4.** Electrospray mass spectral nitrate ($m/z = -62$) signal intensities detected on microjets of deionized H_2O, 1-mM NaCl/H_2O, D_2O, and 1-mM NaCl/D_2O exposed to 4-ppbv gaseous nitric acid for approximately 10 μs at pH of approximately 8. It is apparent that the extent of dissociation of gaseous nitric acid is nearly independent of reactant or solvent deuteration KIEs. All experiments in 1 atm of $N_{2(g)}$ at 293 K.
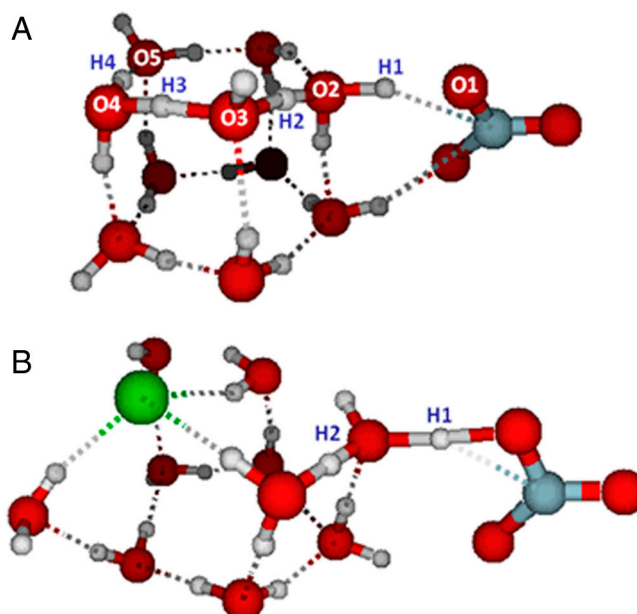

Fig. S5. (*A*, *B*) Schematics of TS for PT on water cluster in absence and presence of interfacial chloride. The internal reaction coordinate with the TS of Fig. 3*A* is a combination of six O—H internal modes, whereas in the presence of chloride (Fig. 3*B*) the TS only involves motions of the H atoms being transferred along the proton wire. While the preorganization of the surface of water in presence of chloride en route to TS leads to minimal requirement on the motion of heavy oxygen atoms, in its absence the TS imaginary mode requires movements of the heavy oxygen atoms to accommodate PT (see animations at http://www.wag.caltech.edu/catalysis/projects/PT.html).